Numerical Analysis of Crystal Growth of an InAs-GaAs Binary Semiconductor under Microgravity Conditions

Yoshiaki Hiraoka†, Keisuke Ikegami†, Toru Maekawa†
Satoshi Matsumoto††

† Toyo University
†† National Space Development Agency of Japan

We investigate the possibilities of growing a uniform binary compound crystal in space numerically, proposing a new crystal growth method. We develop a numerical calculation method of the growth of binary crystals, in which convection induced by temperature and concentration differences in the solution is taken into account. How to determine the shape and movement of the solution–crystal interface during the crystal growth is clearly explained for binary crystals, which is more complicated than that for single-component crystals. The boundary fit method is employed to solve this moving boundary phase transition problem. The calculation method is applied to the crystal growth analysis of an InAs-GaAs binary semiconductor and the effect of buoyancy convection induced under microgravity conditions on the crystal growth process is investigated. We found that the concentration field is disturbed and, as a result, the solution–crystal interface is deformed by buoyancy convection even when the gravitational acceleration is as low as 10^{-6} g, which is supposed to be the gravity level in the International Space Station. We also found that the direction of residual gravity has a strong effect on the concentration field in the solution and the crystal growth process. Next, we analyse the influence of g-jitters and the Sorét effect on the crystal growth process. We, in fact, found that g-jitters and the Sorét effect have little influence on the macroscopic crystal growth process. The dependence of the generation of supercooling in the solution on convection is also investigated. We found that supercooling is not induced by convection if residual gravity is 10^{-6}g. Finally, the possibility of growing high quality InGaAs crystals of uniform compositions in space is discussed.

1. Introduction

One of the factors which determine the quality of grown crystals may be convective instabilities induced in the melt or solution during the crystal growth process. Growing a multi-component semiconductor crystal which has a uniform composition is especially difficult from both fluid dynamical and thermodynamical points of view [1-6]. Therefore, microgravity experiments of crystal growth have been intensively carried out using microgravity experimental facilities such as drop towers, aircraft, rockets, space shuttles and satellites in recent years in order to reduce buoyancy convection and grow high quality crystals [7,8]. We carried out a microgravity experiment of InP crystal growth using an experimental satellite called the Space Flyer Unit (SFU) in 1995 [9,10]. The level

This document is provided by JAXA.

of the residual gravity was 10^{-5}g. The length of the InP single crystal grown by the travelling heater method on earth was 2.6 mm, whereas that of the space grown crystal was 5.7 mm. Although a longer crystal was grown in space, the interface became wavy and the crystal was polycrystallised during the crystal growth process. As we mentioned, a great number of crystal growth experiments have been carried out under microgravity conditions, but not many high quality single crystals of uniform compositions have been grown. Striations often formed in the grown crystals.

Although it is commonly believed that the quality of crystals is directly related to convection induced in the melt or solution, the effect of convection on the crystal growth process has not yet been completely understood. It is impossible to grow high quality compound crystals by experience, unlike single-component crystals. There are two main points which make the growth of multi-component crystals more difficult and complicated compared to the growth of single-component crystals: (1) The shape and movement of the solution–crystal interface are determined by the concentration field in addition to the velocity and temperature fields. The interfacial temperature and concentration of the solute vary along the solution–crystal interface. Note that the interfacial temperature is the melting temperature and therefore is constant along the interface in the case of single-component crystals. (2) Concentration of the solute at the crystal side of the interface is different from that at the solution side of the interface, which is determined by the liquidus and solidus curves on the phase diagram. Solute is ejected from the crystal into the solution and latent heat is released as phase transition progresses. Since concentration becomes high near the interface in the solution, supercooling tends to occur, which may cause polycrystallisation.

There is a demand for single high quality compound crystals to be grown as future materials for fast and efficient electronic or optical devices [11]. $In_XGa_{1-X}As$ has great potential as a future laser since the wavelength can be altered by changing the composition X. Especially, when X = 0.3, a laser of wavelength 1.3 μm, which transmits data through a quartz fibre most efficiently, can be produced [11]. However, it is almost impossible to grow $In_{0.3}Ga_{0.7}As$ crystals on earth due to strong buoyancy convection and sedimentation. Note that the gap between the solidus and liquidus curves is very wide at X = 0.3 (see figure 3 for the phase diagram), which makes crystal growth extremely difficult. In this report, we develop a calculation method of the growth of binary crystals and analyse the crystal growth process of an InAs-GaAs binary semiconductor. In section 2, we summarise an idea of growing a uniform $In_{0.3}Ga_{0.7}As$ crystal, utilising microgravity conditions. In section 3, we develop a calculation method for estimating the flow, temperature and concentration fields and the shape and movement of the solution–crystal interface. In section 4, we analyse the growth process of an InAs-GaAs binary crystal and make clear the effect of buoyancy convection and the direction of residual gravity on the crystal growth process. We also investigate the influence of g-jitters and the Sorêt effect on the crystal growth process. Finally, we discuss the possibilities of growing uniform $In_{0.3}Ga_{0.7}As$ crystals in space. In the final section, we summarise the results obtained through the analyses.

2. New method of growing uniform binary crystals

Generally speaking, when the initial concentration distribution of the solute is uniform throughout the solution, the concentration in the grown crystal decreases in the early stage and, after that, increases as the crystal grows. In other words, the compositions of the grown crystal are not uniform. If the initial concentration of the solute has a positive gradient in the solution towards the growing crystal, a crystal of uniform compositions may grow. We call this technique 'Graded Solute Concentration method' which is abbreviated to the 'GSC method' [12,13]. The initial concentration distribution does not remain on earth because of strong buoyancy convection. However, it can be maintained in microgravity. We investigated the dependence of the relaxation time of concentration on the microgravity

This document is provided by JAXA.

level [14]. The relaxation time is over 1000 s if the residual gravity is 10^{-4} g and even if the temperature gradient is as high as 100 K/cm. This new crystal growth technique is described in figure 1 and summarised in the following; (1) We grow InGaAs under 1g conditions. In this case, the concentration distribution of InAs in the grown crystal is not uniform (figure 1(a)). (2) The grown crystal is heated to become a solution in microgravity. As we mentioned, the initial concentration distribution in the solution is maintained under microgravity conditions. We start growing a crystal in the opposite direction (figure 1(b)). We carried out one-dimensional crystal growth analysis under zero gravity and found that it is possible to grow $In_{0.3}Ga_{0.7}As$ by setting a high temperature gradient and controlling the heater speed [12]. However, we are not sure whether it is possible to grow $In_{0.3}Ga_{0.7}As$ under 10^{-6} g conditions, which is believed to be the gravity level in the International Space Station.

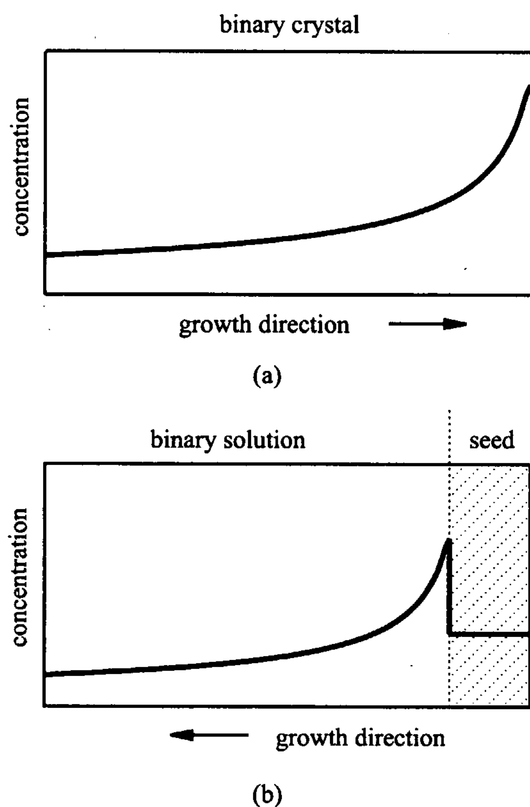

Figure 1 New crystal growth technique utilising microgravity conditions.

(a) A binary crystal is grown under terrestrial gravity conditions. The concentration of the solute increases in the growth direction in this case.

(b) The earth grown crystal is heated to become a solution in microgravity. The initial concentration distribution is maintained under microgravity conditions. Crystal growth starts in the opposite direction. We expect the concentration to remain constant, without any decrease, in the early stage and to become uniform in most of the grown crystal.

3. Numerical modelling of binary crystal growth

In this section, we develop a numerical model and introduce the governing equations of the growth of binary crystals. An outline of our numerical model of InAs-GaAs crystal growth is shown in figure 2. The calculation area is divided into three regions; that is, single crystal, solution and container wall. The solution and the crystal are placed in a two-dimensional container. The heat flux at the outer surface of the container is given externally as shown in figure 2, which is based on the heater of the crystal growth experimental system of the Japanese Experimental Module (JEM) in the International Space Station. The top and bottom surfaces are heated and the right- and left-hand side walls are, respectively, cooled and thermally isolated. The total amount of the heat input is equal to that of the heat output. The heaters move to the left, that is, in the $-x_1$ direction so that the crystal grows in the $-x_1$ direction. The solution–crystal interface is expressed by the following equation; $x_1 = F(x_2, t)$, which is a function of time, t, and the coordinate, x_2, and is determined by the heat and mass balance at the interface and the liquidus and solidus curves on the phase diagram as long as the local equilibrium holds at the interface. The governing equations are summarised in the following.

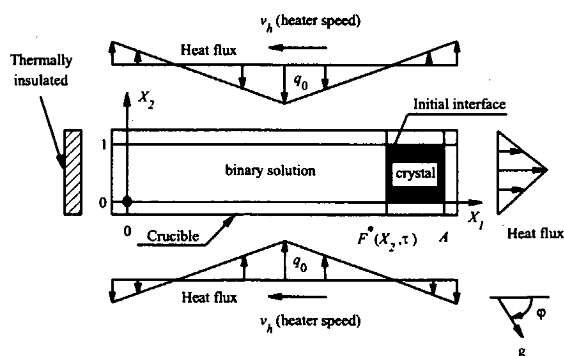

Figure 2 Numerical model of two-dimensional InAs-GaAs crystal growth.

This document is provided by JAXA.

The coordinate x_i, time t, pressure p, velocity u_i and temperature T are nondimensionalised as follows:

$$X_i \equiv \frac{x_i}{L},\ \tau \equiv \frac{t}{L^2/\nu_L},\ U_i \equiv \frac{u_i}{\nu_L/L}$$
$$P \equiv \frac{p}{\rho_0 \nu_L^2/L^2},\ \theta \equiv \frac{T-T_f}{q_0 L/\lambda_L} \tag{1}$$

where L, ν, ρ_0, q_0 and λ are, respectively, the depth of the solution layer, the kinematic viscosity, the density, the maximum value of the heat flux (see figure 2) and the thermal conductivity. Subscripts L, S and f represent liquid, solid and the melting point of InAs. Note that the concentration of InAs is already nondimensionalised (see figure 3). The nondimensional governing equations are shown in the following.

3.1 Governing equations in solution

The Boussinesq approximation being applied to the density change, the continuity, momentum and heat and concentration transport equations are expressed as follows:

Continuity equation;

$$\frac{\partial U_i}{\partial X_i} = 0 \tag{2}$$

Momentum equation;

$$\frac{\partial U_i}{\partial \tau} + U_j \frac{\partial U_i}{\partial X_j} = -\frac{\partial P}{\partial X_i} + \frac{\partial^2 U_i}{\partial X_j \partial X_j} + \frac{Ra^T}{Pr}\theta_L k_i - \frac{Ra^C}{Sc} C_L k_i \tag{3}$$

where the buoyancy forces based on both the temperature and concentration differences are taken into account (the third and fourth terms on the right-hand side) and k_i is the unit vector in the gravitational direction. In the case of the InAs-GaAs system, the density increases with a decrease in temperature and with an increase in the concentration of InAs.

Energy equation;

$$\frac{\partial \theta_L}{\partial \tau} + U_j \frac{\partial \theta_L}{\partial X_j} = \frac{1}{Pr}\frac{\partial^2 \theta_L}{\partial X_j \partial X_j} \tag{4}$$

Transport equation of concentration of InAs;

$$\frac{\partial C_L}{\partial \tau} + U_j \frac{\partial C_L}{\partial X_j} = \frac{1}{Sc}\frac{\partial^2 C_L}{\partial X_j \partial X_j} \tag{5}$$

Ra^T, Ra^C, Pr and Sc appearing in the above equations are, respectively, the Rayleigh number based on the temperature, the Rayleigh number based on the concentration, the Prandtl number and the Schmidt number.

$$Ra^T \equiv \frac{\beta g q_0 L^4}{\lambda_L \kappa_L \nu_L},\ Ra^C \equiv \frac{\gamma g \Delta C L^4}{D_L \nu_L}$$
$$Pr \equiv \frac{\nu_L}{\kappa_L},\ Sc \equiv \frac{\nu_L}{D_L} \tag{6}$$

where β, g, κ_L, γ and D_L are, respectively, the temperature coefficient of volume expansion, the gravitational acceleration, the thermal diffusivity, the concentration coefficient of volume expansion and the diffusion coefficient.

3.2 Governing equations in crystal

In the crystal, the governing equations are the heat conduction and concentration diffusion equations since convection does not need to be taken into account.

Heat conduction equation;

$$\frac{\partial \theta_S}{\partial \tau} = \frac{K_{SL}}{Pr}\frac{\partial^2 \theta_S}{\partial X_j \partial X_j} \tag{7}$$

Diffusion equation;

$$\frac{\partial C_S}{\partial \tau} = \frac{D_{SL}}{Sc}\frac{\partial^2 C_S}{\partial X_j \partial X_j} \tag{8}$$

K_{SL} is the ratio of the thermal diffusivity of the crystal to that of the solution and D_{SL}, the ratio of the diffusion coefficient in the crystal to that in the solution.

$$K_{SL} \equiv \frac{\kappa_S}{\kappa_L},\ D_{SL} \equiv \frac{D_S}{D_L} \tag{9}$$

The heat conduction equation in the container walls must also be solved with the above equations (2)-(5), (7) and (8).

3.3 Solution–crystal interface

The temperature and concentration at the solution–crystal interface and the position of the interface are determined by the heat and mass balance at the interface and the liquidus and solidus curves on the

This document is provided by JAXA.

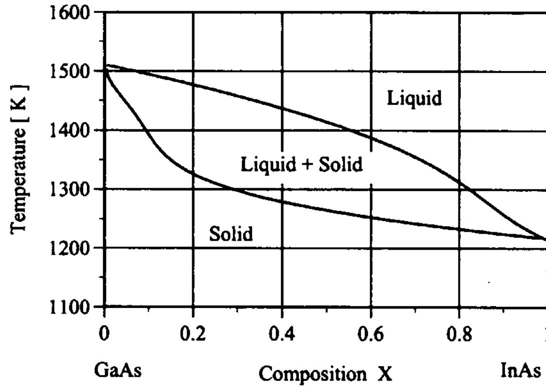

Figure 3 Pseudo-binary phase diagram of $In_XGa_{1-X}As$.

phase diagram. The phase diagram of the InAs-GaAs binary system is shown in figure 3 [3].

Heat balance at the interface;

$$\frac{\partial F^*}{\partial \tau} = \frac{Sf}{Pr}\left\{-\left(\frac{\partial \theta_L}{\partial X_1} - \frac{\partial F^*}{\partial X_2}\frac{\partial \theta_L}{\partial X_2}\right) + G_{SL}\left(\frac{\partial \theta_S}{\partial X_1} - \frac{\partial F^*}{\partial X_2}\frac{\partial \theta_S}{\partial X_2}\right)\right\} \tag{10}$$

Mass balance at the interface;

$$\left(C_L - C_S\right)\frac{\partial F^*}{\partial \tau} = \frac{1}{Sc}\left\{-\left(\frac{\partial C_L}{\partial X_1} - \frac{\partial F^*}{\partial X_2}\frac{\partial C_L}{\partial X_2}\right) + D_{SL}\left(\frac{\partial C_S}{\partial X_1} - \frac{\partial F^*}{\partial X_2}\frac{\partial C_S}{\partial X_2}\right)\right\} \tag{11}$$

where F^* is the position of the solution–crystal interface nondimensionalised by L, G_{SL}, the ratio of the thermal conductivity of the crystal to that of the solution, and Sf, the Stefan number.

$$G_{SL} \equiv \frac{\lambda_S}{\lambda_L},\ Sf \equiv \frac{q_0 L}{\rho_0 L_{SL} \kappa_L} \tag{12}$$

Here, L_{SL} is the latent heat per unit mass.

There is one important point which we must take into account; that is, the temperature and concentration are not independent at the solution–crystal interface. The relation between the temperature and the concentration is given by the liquidus and solidus curves on the phase diagram. Temperature changes continuously at the interface and therefore the temperatures, θ_L and θ_S, are the same at the interface, whereas concentration C_L is different from C_S at the interface. Once the interfacial temperature is assigned, C_L and C_S at the interface are determined by the liquidus and solidus curves.

$$C_L = f_L(\theta_L),\ C_S = f_S(\theta_S) \tag{13}$$

where functions f_L and f_S represent the liquidus and solidus curves, respectively. Note that $\theta_L = \theta_S$ at the interface as we mentioned. In the present analysis, we approximated the liquidus and solidus curves, f_L and f_S, by polynomial functions of the fifth-order. Since $\partial F^*/\partial \tau$ is common in equations (10) and (11), the right-hand side of equation (10) is equal to the right-hand side of equation (11) divided by $(C_L - C_S)$. Therefore, the interfacial temperature can be calculated. The interfacial temperature having been determined, the concentrations at the interface are obtained by equation (13).

There is another important point; that is, the interfacial energy of the solution–crystal interface. The phase diagram is applicable to planar interfaces. Once the interface is deformed, which usually occurs during the crystal growth process, the interfacial energy must be taken into account to determine the interfacial temperature. Taking the Gibbs-Thomson effect into account, the true temperature at the interface is calculated as follows [15]:

$$\theta_L = f_L^{-1}(C_L) - \sigma K \tag{14}$$

where f_L^{-1} is the inverse function of f_L (see equation (13)), K, the curvature of the interface nondimensionalised by L, and σ, the nondimensional interfacial energy which is defined below:

$$\sigma \equiv \frac{\gamma_{SL} \lambda_L T_f}{\rho_0 L_{SL} q_0 L^2} \tag{15}$$

Here, γ_{SL} is the interfacial tension.

3.4 Numerical method and procedure

Since the solution–crystal interface moves and the interfacial shape changes during the crystal growth process, we employ the boundary fit method to solve the governing equations efficiently [16]. The governing equations are transformed introducing the following new coordinates ξ and η:

This document is provided by JAXA.

$$\xi \equiv \frac{X_1}{F^*(X_2,\tau)} \qquad \text{(solution)} \qquad (16)$$

$$\eta \equiv \frac{X_1 - F^*(X_2,\tau)}{A - F^*(X_2,\tau)} \qquad \text{(crystal)} \qquad (17)$$

where A is the aspect ratio of the container (see figure 2). ξ and η are normalised as $0 \leq \xi \leq 1$, $0 \leq \eta \leq 1$. The transformed governing equations are solved by the finite difference method. The time and spatial derivatives are approximated by the first-order explicit formula and the second-order central formula, respectively.

Now, we can calculate the crystal growth process, that is, the velocity, temperature and concentration fields and the shape and movement of the solution–crystal interface. The numerical procedure is as follows:

(1) We place the solution and crystal in the container. The interface is planar initially.

(2) The initial concentration of InAs in the seed crystal is 0.3 and that in the solution is calculated based on the complete mixing theory [17]. Note that we employ the GSC method which is explained in section 2. The average concentration in the solution is 0.3 initially. The initial concentration distribution is shown in figure 4.

(3) We start heating and cooling the system externally as shown in figure 2.

(4) We solve the governing equations in the solution, crystal and container wall (see sections 3.1 and 3.2).

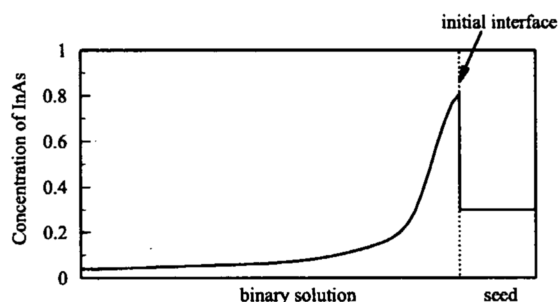

Figure 4 Initial concentration distribution of InAs. Concentration in the solution is calculated by the complete mixing theory and the average concentration in the solution is 0.3.

(5) The interfacial temperature and concentrations are determined by the heat and mass balance equations at the interface and the phase diagram (see section 3.3).

(6) The interfacial temperature having been determined, the time derivative of the solution–crystal interface is calculated by equation (10). Therefore, the new position of the interface is obtained.

(7) The new interfacial shape having been obtained, the curvature of the interface is calculated and the interfacial temperature is modified by equation (14).

(8) Using the new interfacial temperature, we solve the governing equations.

Procedures (4)-(8) are repeated.

The nondimensional parameters were estimated based on the physical properties of InAs and GaAs [18,19]. The residual gravity is 10^{-6}g. The depth of the container, the length of the container, and the thickness of the wall are, respectively, 20 mm, 120 mm and 5 mm. The container wall is made of quartz glass. The initial concentration distribution is shown in figure 4 and the initial temperature gradient is 40 K/cm in the solution and 60 K/cm in the crystal. The maximum heat flux, q_0, is changed from 1.0 to 5.0 kW/m^2 and the heater speed is changed from 0.25 to 2.0 mm/h. The physical properties, system dimensions and growth conditions are summarised in table 1.

The calculation space was divided by 72×41, 92×61 and 112×81 finite difference grids and the maximum differences in the stream function, temperature, concentration and positions of the interface caused by the differences in the number of the finite difference grid points were within 3 %. The results shown in the following are based on the calculations using 92×61 grid points.

4. Result and discussion

We investigate the influence of the direction of residual gravity, the depth of the solution layer, the heat flux, the heater speed, g-jitters and the Sorét effect on the velocity, temperature and concentration fields, the shape and movement of the solution–crystal interface and the generation of supercooling

This document is provided by JAXA.

Table 1 Physical properties, system dimensions and growth conditions

Kinematic viscosity	ν_L	[m^2 s^{-1}]	3.0×10^{-7}
Density	ρ_0	[kg m^{-3}]	5.9×10^3
Thermal conductivity of solution	λ_L	[W m^{-1} K^{-1}]	3.0
Thermal conductivity of crystal	λ_S	[W m^{-1} K^{-1}]	1.2
Thermal conductivity of container	λ_C	[W m^{-1} K^{-1}]	3.0
Temperature coefficient of volume expansion	β	[K^{-1}]	1.83×10^{-4}
Concentration coefficient of volume expansion	γ	[-]	3.84×10^{-2}
Thermal diffusivity of solution	κ_L	[m^2 s^{-1}]	1.2×10^{-6}
Thermal diffusivity of crystal	κ_S	[m^2 s^{-1}]	0.6×10^{-6}
Thermal diffusivity of container	κ_C	[m^2 s^{-1}]	1.6×10^{-7}
Diffusion coefficient of In in solution	D_L	[m^2 s^{-1}]	1.0×10^{-8}
Diffusion coefficient of In in crystal	D_S	[m^2 s^{-1}]	1.0×10^{-11}
Latent heat	L_{SL}	[J kg^{-1}]	5.0×10^5
Interfacial tension	$\gamma_{SL} T_f / \rho_0 L_{SL}$	[K m]	1.0×10^{-7}
Sorét coefficient	χ / T_L	[1/K]	2.0×10^{-4}
Depth of solution and crystal	L	[mm]	10, 15, 20
Width of solution and crystal	W	[mm]	120
Thickness of wall	d	[mm]	5
Maximum heat flux	q_0	[kW m^{-2}]	1.0, 3.0, 5.0
Heater speed	ν_h	[mm h^{-1}]	0.25, 0.5, 1.0, 2.0

in the solution.

First, we analyse the effect of the gravitational direction on the crystal growth process. The streamlines, isotherms, isoconcentration lines and the interfacial shape are shown in figure 5 where residual gravity acts in the perpendicular to the solution layer (figure 5(a)) and in parallel to the solution layer (figure 5(b)). The temperature field is not deformed seriously in either case since the Prandtl number is very small. However, when the container is placed horizontally, the concentration field is disturbed by buoyancy convection and, as a result, the solution–crystal interface is deformed even when residual gravity is as low as 10^{-6}g (figure 5(a)). When the container is placed vertically, on the other hand, both temperature and concentration fields are not disturbed by buoyancy convection and therefore the solution–crystal interface is almost flat since the system is thermally stable (figure 5(b)). The time variations of the interfacial shape and movement are shown in figure 6 for both horizontal and vertical cases. Crystal grows faster and the deformation of the interface becomes more serious in the horizontal case (figure 6(a)) than in the vertical case (figure 6(b)). The time variation of the maximum convective velocity in the solution is shown in figure 7 for the vertical and horizontal cases. Convection is reduced remarkably when crystal grows in the antigravitational direction since the system is thermally stable.

As the Schmidt number is large; in other words, the diffusion coefficient is small, the concentration is transported mainly by convection. As heat is removed from the right-hand side wall, liquid near the crystal is cooled. Since In is ejected from the crystal into the solution as the crystal grows, the concentration of In is high near the solution–crystal interface. Since the density of the solution increases with a decrease in the temperature and with an increase in the concentration of In, clockwise convection is induced in the horizontal case (see figure 5(a)). Therefore, In is transported to the lower part of the solution and the concentration of In becomes high in the lower part of the solution near the solution–crystal interface

This document is provided by JAXA.

(figure 5(a)), which slows the growth rate of the lower part of the crystal (see equation (11) and figures 5(a) and 6(a)). As the system is thermally stable in the vertical case, convection is very weak and, as a result, the crystal growth rate is low and the interfacial shape is almost flat. Even under microgravity conditions, the direction of residual gravity has a strong influence on the growth process of binary crystals, which is, in fact, not always taken into account in the crystal growth experiments in microgravity.

We checked the size effect on the crystal growth process by changing the depth of the solution layer in the horizontal case. The streamlines and the interfacial shape are shown in figure 8 where residual

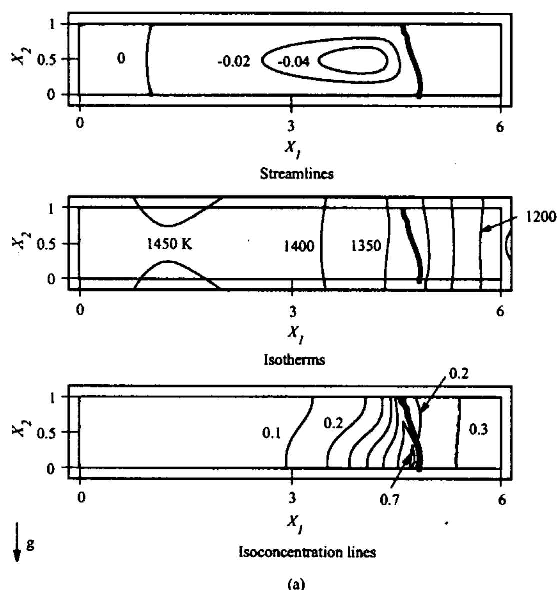

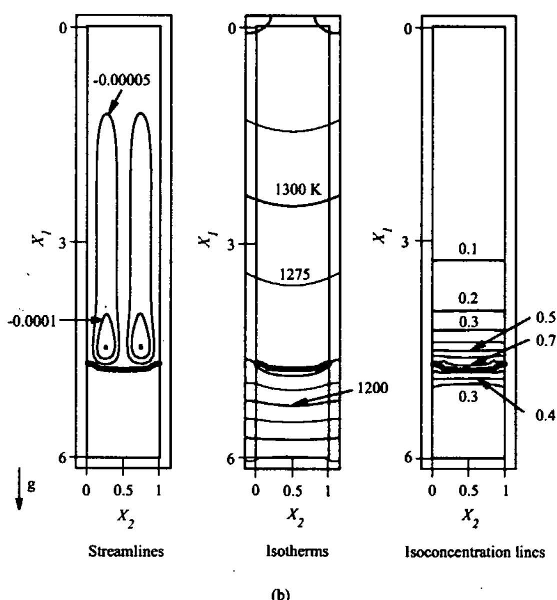

Figure 5 Streamlines, isotherms, isoconcentration lines and interfacial shape. $Ra^T = 0.78$, $Ra^C = 1000$, $Pr = 0.18$, $Sc = 30$, $Sf = 0.0672$, $\sigma = 3.3 \times 10^{-9}$, v_h (heater speed) = 1.0 mm/h, $q_0 = 3.0$ kW/m^2. The thick curve represents the solution–crystal interface.
(a) The container is placed horizontally. $\tau = 4.0$.
(b) The container is placed vertically. $\tau = 40.0$.

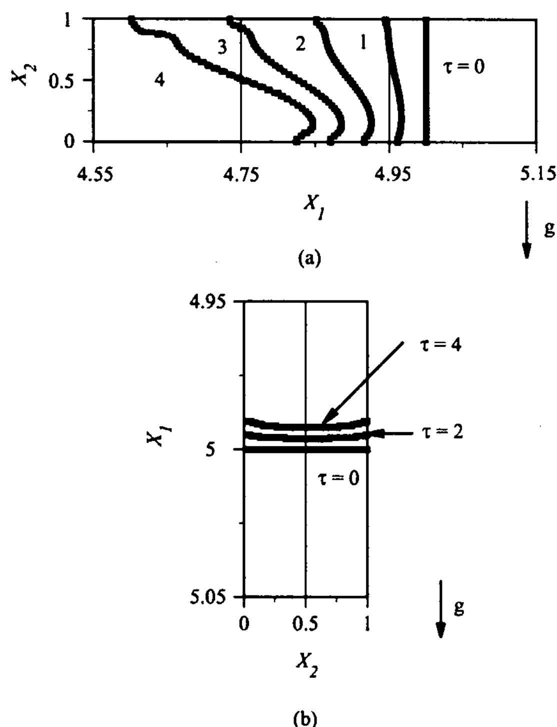

Figure 6 Time variation of interfacial shape and movement. $Ra^T = 0.78$, $Ra^C = 1000$, $Pr = 0.18$, $Sc = 30$, $Sf = 0.0672$, $\sigma = 3.3 \times 10^{-9}$, $v_h = 1.0$ mm/h, $q_0 = 3.0$ kW/m^2.
(a) The container is placed horizontally.
(b) The container is placed vertically.

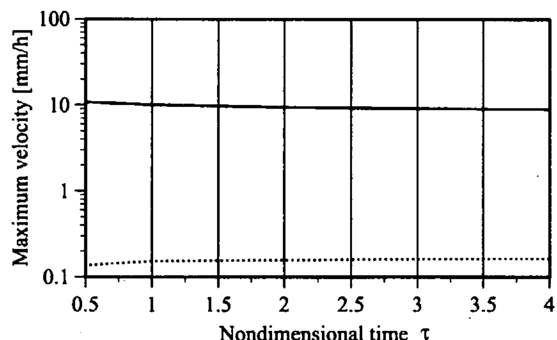

Figure 7 Time variation of maximum convective speed in solution. $Ra^T = 0.78$, $Ra^C = 1000$, $Pr = 0.18$, $Sc = 30$, $Sf = 0.0672$, $\sigma = 3.3 \times 10^{-9}$, $v_h = 1.0$ mm/h, $q_0 = 3.0$ kW/m^2.
——— : Horizontal case ········ : Vertical case.

This document is provided by JAXA.

gravity acts in the perpendicular to the solution layer and the depth of the solution layer is 10 mm, 15 mm and 20 mm. As the crystal size increases, convection becomes noticeable and the solution–crystal interface is deformed. The time variation of the maximum velocity in the solution is shown in figure 9. As the crystal size increases, velocity increases. Growth of a large scale compound crystal is still difficult even in space.

Next, we investigate the effect of the heater power and the heater speed on the growth process in the horizontal case. The time variation of the solution–crystal interface is shown in figure 10 where the maximum heat flux, q_0 (see figure 2), is 1.0 kW/m^2 (figure 10(a)), 3.0 kW/m^2 (figure 10(b)) and 5.0 kW/m^2 (figure 10(c)). As is expected, convection becomes stronger and the deformation of the interface becomes more serious as the heat flux increases. Note that since the amount of heat input is balanced with that of heat output, the crystal growth rate becomes higher as the heat flux increases. On the other hand, the effect of the heater speed on the growth process was not so noticeable. The dependence of the maximum velocity in the solution on the heat flux and the heater speed is shown in figure 11. The velocity increases with the heater power as we mentioned, but the velocity is almost constant despite the heater speed differences as long as the heater speed lies between 0.5 and 2.0 mm/h.

It is often mentioned that g-jitters [20] and the Sorét effect [21,22] may seriously affect the crystal growth

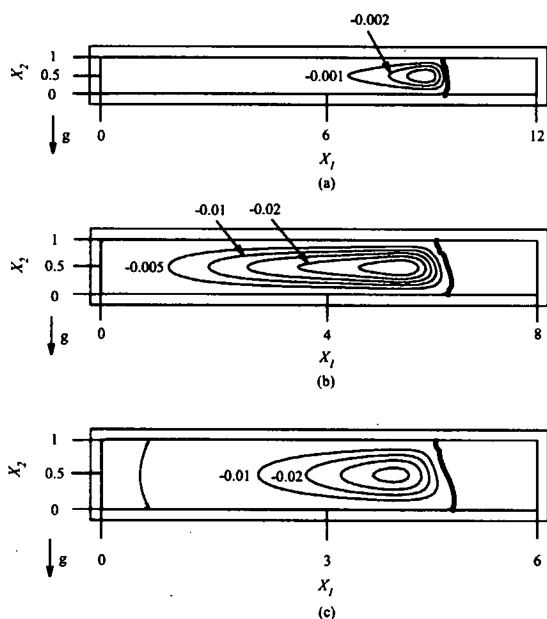

Figure 8 Streamlines and interfacial shape. $Pr = 0.18$, $Sc = 30$, $v_h = 1.0$ mm/h, $q_0 = 2.0$ kW/m^2.
(a) The depth of the solution and crystal, L, is 10 mm. $\tau = 11.0$
(b) $L = 15$ mm. $\tau = 6.5$
(c) $L = 20$ mm. $\tau = 5.0$

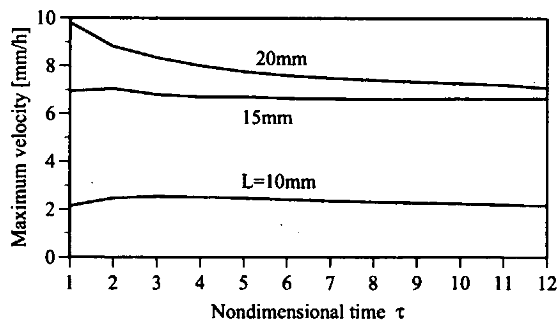

Figure 9 Time variation of maximum convective speed in solution. The dependence of the maximum velocity on the depth of the solution is shown. $Pr = 0.18$, $Sc = 30$, $v_h = 1.0$ mm/h, $q_0 = 2.0$ kW/m^2.

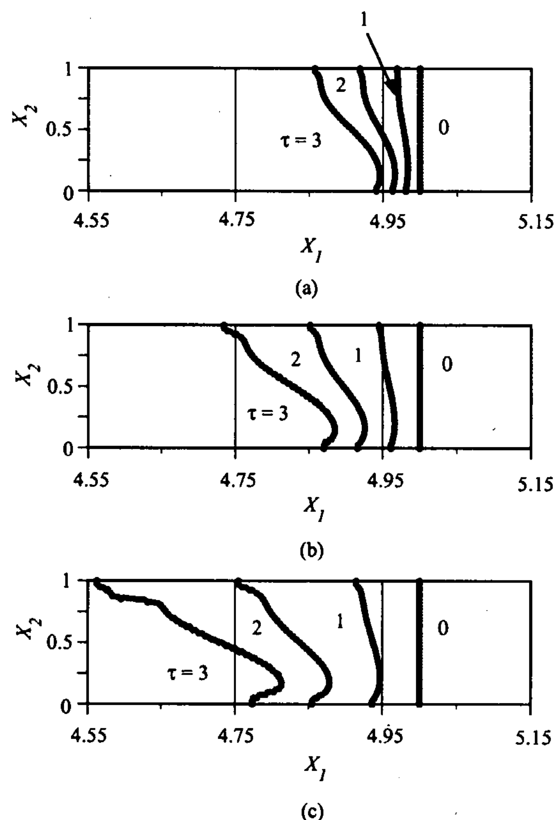

Figure 10 Time variation of interfacial shape and movement. $Ra^C = 1000$, $Pr = 0.18$, $Sc = 30$, $v_h = 1.0$ mm/h.
(a) $q_0 = 1.0$ kW/m^2. (b) $q_0 = 3.0$ kW/m^2. (c) $q_0 = 5.0$ kW/m^2.

This document is provided by JAXA.

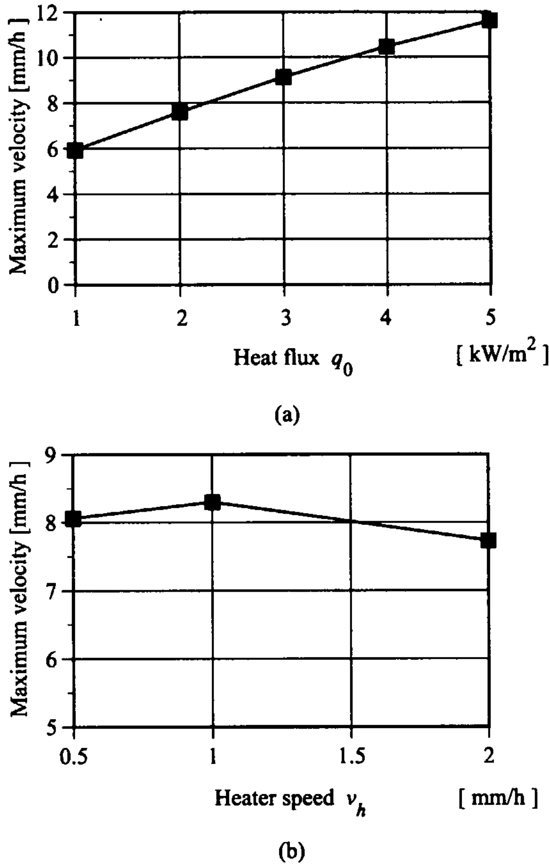

Figure 11 Dependence of maximum velocity on heat flux and heater speed.
(a) Dependence on heat flux.
(b) Dependence on heater speed.

process in microgravity, but the idea has not yet been proved. Therefore, we investigated the effect of g-jitters on the crystal growth process by altering residual gravity sinusoidally with time. The following terms were added on the right-hand side of the momentum equation (3).

$$\left(\frac{Ra^T_{jitter}}{Pr} \theta_L - \frac{Ra^C_{jitter}}{Sc} C_L \right) sin(\Omega\tau)\, k_i \tag{18}$$

where Ra^T_{jitter}, Ra^C_{jitter} and Ω are defined as follows:

$$Ra^T_{jitter} \equiv \frac{\beta g_A q_0 L^4}{\lambda_L \kappa_L \nu_L}, \quad Ra^C_{jitter} \equiv \frac{\gamma g_A \Delta C L^3}{D_L \nu_L}$$
$$\Omega \equiv \frac{2\pi f}{\nu_L / L^2} \tag{19}$$

Here, g_A and f are, respectively, the amplitude and frequency of g-jitter. We carried out simulations for (g_A, f) = (10^{-6}g, 0.01 Hz), (10^{-5}g, 0.1 Hz), (10^{-4}g, 1.0 Hz) and (10^{-3}g, 10 Hz), which are the estimated combinations of the amplitude and frequency of g-jitters in the International Space Station. However, no noticeable g-jitter effects on the crystal growth process were detected from a macroscopic point of view in this analysis. As the direction of g-jitters usually changes with time, we still need to investigate the effect of the time variation of the g-jitter directions on the crystal growth process by three- as well as two-dimensional calculations in the future. Although the effect of g-jitters on the macroscopic crystal growth process was negligible in the present analysis, the microstructures of the grown crystal may still be altered by the temperature and concentration fluctuations [23,24].

Next, we checked the Sorét effect on the crystal growth process. To take the Sorét effect into account, we changed the right-hand side term of the transport equation of InAs in the solution as follows (see equation (5)):

$$\frac{1}{Sc}\left(\frac{\partial^2 C_L}{\partial X_j \partial X_j} + \Gamma \frac{\partial^2 \theta_L}{\partial X_j \partial X_j} \right) \tag{20}$$

where Γ is the parameter which represents the Sorét effect.

$$\Gamma \equiv \frac{\chi q_0 L}{T_L \lambda_L} \tag{21}$$

Here, χ / T_L is the Sorét coefficient. Since the Sorét coefficient of InAs in the InGaAs solution has not yet been measured, we estimated the Sorét parameter based on the Sorét coefficient of Ga in the GaAs solution [21]. The distributions of the concentration of InAs at the centre of the container along the horizontal axis is shown in figure 12. The dashed curve indicates the concentration distribution when the Sorét coefficient, which is 1000 times larger than the normal value, is assigned. The concentration field is not altered by the Sorét effect although it is slightly affected in the solution when the unnecessarily large value is given.

Finally, we investigated supercooling occurring in the solution. The area where the local concentration is higher than the saturation concentration corresponding to the local temperature is supersaturated or supercooled. We defined the degree of supercooling, S, as follows [25,26]:

This document is provided by JAXA.

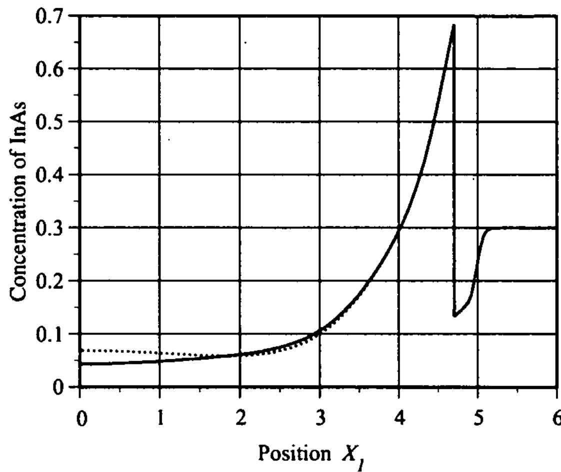

Figure 12 Concentration distribution. The influence of the Sorét effect on the concentration distribution is shown.
—— : $\chi/T_L = 0$; The Sorét effect is not taken into account.
········ : $\chi/T_L = 2.0 \times 10^{-1}$; χ/T_L is 1000 times greater than the normal value.

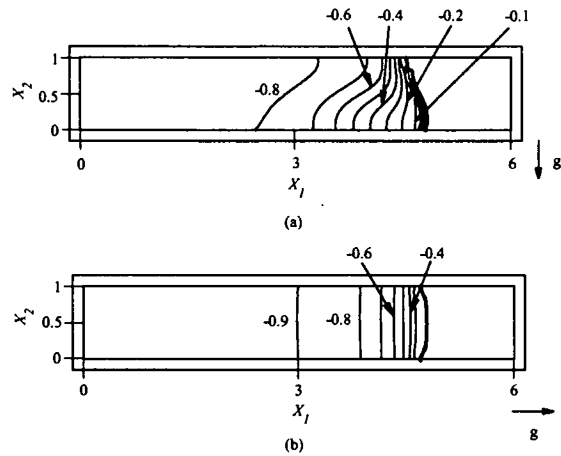

Figure 13 Distribution of degree of supercooling S. $Ra^T = 0.78$, $Ra^C = 1000$, $Pr = 0.18$, $Sc = 30$, $Sf = 0.0672$, $\sigma = 3.3 \times 10^{-9}$, $v_h = 1.0$ mm/h, $q_0 = 3.0$ kW/m^2. S is defined by equation (22).
(a) The container is placed horizontally. $\tau = 4.5$.
(b) The container is placed vertically. $\tau = 40.0$.

$$S \equiv \frac{C_L - C_{L,sat}}{C_{L,sat}} \tag{22}$$

where C_L is the local concentration in the solution and $C_{L,sat}$, the saturation concentration corresponding to the local temperature. The area where S is positive is supercooled. The distribution of S is shown in figure 13. Since the concentration of In becomes high in the lower part of the solution near the crystal in the horizontal case (see figure 5(a)), supercooling may occur in the area. However, in either vertical and horizontal case, supercooling is not induced by the buoyancy convection. In that sense, convection induced under 10^{-6}g is weak. On the contrary, strong supercooling occurs in the solution under terrestrial gravity conditions due to strong buoyancy convection [25,26], which may cause polycrystallisation. Because of the suppression or reduction of supercooling in the solution as well as sedimentation, microgravity conditions are necessary for the crystal

However, it is still difficult to grow compound crystals of uniform compositions even under microgravity conditions as we have demonstrated. According to our analysis, crystal should be grown in the antigravitational direction. In this case, we found that the heater speed; 0.25 mm/h, and the heat flux, q_0; 5 kW/m^2, are the best conditions for the production of $In_{0.3}Ga_{0.7}As$ (see figure 14). The shape

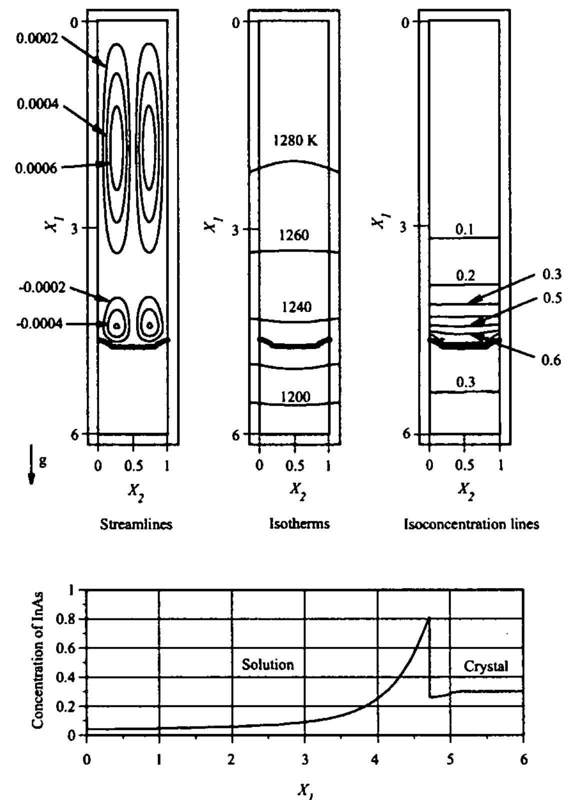

Figure 14 Streamlines, isotherms, isoconcentration lines, interfacial shape and concentration distribution along the centre of the container. Crystal is grown in the antigravitational direction. $Ra^T = 1.3$, $Ra^C = 1000$, $Pr = 0.18$, $Sc = 30$, $Sf = 0.112$, $\sigma = 2.0 \times 10^{-9}$, $\tau = 17.0$. Crystal of X = 0.3 can be grown when the heater speed is 0.25 mm/h and the heat flux, q_0, is 5.0 kW/m^2.

This document is provided by JAXA.

of the crystal interface is, however, concave towards the solution, whereas it needs to be convex for the growth of high quality crystals. We are going to investigate the crystal growth process by the zone melt method. In this case, as the solution width is shorter, the reduction of convection may be greater compared to the present case and, as a result, the deformations of the concentration field and the crystal–solution interface may be lessened.

Conclusions

We developed a calculation method of the growth process of binary crystals and investigated the possibilities of growing a uniform binary compound crystal in space, proposing a new crystal growth method. Through the analysis, the following results were obtained: (1) The temperature field is not seriously deformed by convection since the Prandtl number of molten compound semiconductors is very small. (2) The concentration field and the solution–crystal interface are deformed by buoyancy convection even in microgravity when the crystal growth direction is perpendicular to residual gravity since the Schmidt number is large. (3) As the crystal size and the heat flux increase, the deformation of the concentration field and the solution–crystal interface become more serious. (4) The influences of g-jitters and the Sorét effect on the velocity, temperature and concentration fields and the crystal growth process are negligible from a macroscopic point of view. (5) Supercooling is not induced in the solution when residual gravity is as low as 10^{-6}g. (6) A more sophisticated intelligent crystal growth technique is necessary for the production of $In_{0.3}Ga_{0.7}As$; the zone melt method combined with the GSC method may be a more promising technique.

References

[1] Kinoshita K and Sugii K 1984 *J. Crystal Growth* **67** 375-379

[2] Kinoshita K and Sugii K 1985 *J. Crystal Growth* **71** 283-288

[3] Nakajima K, Kusunoki T and Takenaka C 1991 *J. Crystal Growth* **113** 485-490

[4] Kusunoki T, Takenaka C and Nakajima, K 1991 *J. Crystal Growth* **112** 33-38

[5] Baldus A and Benz K W. 1993 *J. Crystal Growth* **130** 37-44

[6] Höschl P, Grill R, Svoboda J, Hlídek P, Moravec P, Franc J and Belas E. 1994 *J. Crystal Growth* **138** 956-963

[7] Walter H U ed 1987 *Fluid Sciences and Materials Science in Space* (Tokyo: Springer-Verlag)

[8] Kodama S, Nakajima K, Suzuki Y, Ohtsuki O and Sakai H. 1988 *J. Crystal Growth* **194** 166-172

[9] Takahashi K, Adachi S and Masaki M 1996 *Proc. Symposium on SFU Experiments for Commercial Utilization* (Tokyo, Japan, 1996) (Tokyo: Institute for Unmanned Space Experiment Free Flyer) pp.75-92, in Japanese

[10] Matsumoto S and Maekawa T 1999 *Int. J. Transport Phenomena* **1** 165-172

[11] Bhattacharya P ed 1993 *Properties of Lattice-Matched and Strained Indium Gallium Arsenide* (London: INSPEC)

[12] Matsumoto S, Maekawa T, Kato K, Yoda S and Kinoshita K 1999 *Adv. Space Res.* **24** 1279-1282

[13] Kinoshita K, Kato H, Matsumoto S and Yoda S 2000 *J. Crystal Growth*, in press

[14] Matsumoto S, Maeda K, Maekawa T, Kato H, Yoda S and Kinoshita K 1996 *J. Jpn. Soc. Microgravity Appl.* **13** .335-336

[15] Coriell S R and McFadden G B 1993 *Morphological Stability* (*Handbook of Crystal Growth Vol.1b Chap.12*) ed Hurle D T J (Amsterdam: North-Holland) pp 785-857

[16] Thompson J F, Warsi Z U A and Mastin C W 1985 *Numerical Grid Generation: Foundations and Applications* (New York: Elsevier)

[17] Tiller W A 1991 *The Science of Crystallization: Macroscopic Phenomena and Defect Generation* (Cambridge: Cambridge University Press)

[18] Glazov V M, Chizhevskaya S N and Glagoleva N N 1969 *Liquid Semiconductors* (New York: Plenum Press)

This document is provided by JAXA.

[19] Hellwege K H ed 1982 *Landolt-Börnstein: Numerical Data and Functional Relationships in Science and Technology* **17** (Berlin: Springer-Verlag)

[20] Koster J N and Sani R L eds 1990 *Low-Gravity Fluid Dynamics and Transport Phenomena* (Washington DC: AIAA)

[21] Rudolph P, Boeck T and Schmidt P 1996 *Cryst. Res. Technol.* **31** 221-229

[22] Zheng L L, Larson D J Jr and Zhang H 1998 *J. Crystal Growth* **191** .243-251

[23] Carlson D J and Witt A F 1991 *J. Crystal Growth* **108** 508-518

[24] Danilewsky A N, Okamoto Y and Benz K W 1992 *Jpn. J. Appl. Phys.* **31** 2195-2201

[25] Matsumoto S, Maekawa T and Takahashi K 1997 *Int. J. Heat Mass Transfer* **40** 3237-3245

[26] Matsumoto S and Maekawa T 1999 *Adv. Space Res.* **24** 1215-1218

This document is provided by JAXA.